RSC Advances

RSC Publishing

PAPER

View Article Online
View Journal | View Issue

Open Access Article. Published on 11 September 2013. Downloaded on 1/20/2026 10:47:54 PM.
This article is licensed under a Creative Commons Attribution 3.0 Unported Licence.

Cite this: *RSC Adv.*, 2013, **3**, 22140

# Far-infrared absorption spectra of synthetically-prepared, ligated metal clusters with $Au_6$, $Au_8$, $Au_9$ and $Au_6Pd$ metal cores†

Jason F. Alvino,[a] Trystan Bennett,[a] David Anderson,[b] Baira Donoeva,[b] Daniil Ovoshchnikov,[b] Rohul H. Adnan,[bc] Dominique Appadoo,[d] Vladimir Golovko,*[b] Gunther Andersson*[e] and Gregory F. Metha*[a]

Received 31st August 2013
Accepted 9th September 2013

DOI: 10.1039/c3ra44803g

**www.rsc.org/advances**

The far infra-red absorption spectra of a series of chemically synthesised, atomically precise phosphine-stabilised gold cluster compounds have been recorded using synchrotron light for the first time. Far-IR spectra of the $Au_6(Ph_2P(CH_2)_3PPh_2)_4(NO_3)_2$, $Au_8(PPh_3)_8(NO_3)_2$, $Au_9(PPh_3)_8(NO_3)_3$, and $Pd(PPh_3)Au_6(PPh_3)_6(NO_3)_2$ clusters reveal a complex series of peaks between 80 and 475 $cm^{-1}$, for which all significant peaks can be unambiguously assigned by comparison with Density Functional Theory (DFT) geometry optimisations and frequency calculation. Strong absorptions in all spectra near 420 $cm^{-1}$ are assigned to the P–$Ph_3$ stretching vibrations. Distinct peaks within the spectrum of each specific cluster are assigned to the cluster core vibrations: 80.4 and 84.1 $cm^{-1}$ ($Au_6$) 165.1 and 166.4 $cm^{-1}$ ($Au_8$), 170.1 and 185.2 $cm^{-1}$ ($Au_9$), and 158.9, 195.2, and 206.7 $cm^{-1}$ ($Au_6Pd$). The positions of these peaks are similar to those observed to occur for the neutral $Au_7$ cluster in the gas phase (*Science*, 2008, **321**, 674–676). Au–P stretching vibrations only occur for $Au_6$ near 420 $cm^{-1}$, although they appear near 180 $cm^{-1}$ for $Au_6Pd$ and involve gold core vibrations.

## Introduction

Over the past decade there has been great interest shown in the size-dependent chemical properties of metal clusters deposited onto active surfaces, particularly with a focus on catalysis. Most of this work has involved the study of size-selected clusters produced in the gas phase and subsequently deposited, or soft-landed, onto appropriately prepared surfaces. For example, Heiz and co-workers were able to utilise this approach to demonstrate that $Au_8$ clusters deposited onto an MgO surface were able to oxidise CO at temperatures as low as 140 K, and also show that smaller clusters were inactive.[1] Less common are studies that involve the preparation of ligand-stabilised metal clusters *via* chemical synthesis, immobilisation of these onto a support, and the subsequent activation of the cluster cores by removal of some, or all, of the ligands. Clearly, a key step with this approach is the careful monitoring of the ligand removal process and to ensure that the clusters remain isolated on the surface (*i.e.* not agglomerated). Using synchrotron-based XPS, we have recently shown that atomically precise phosphine-stabilised gold clusters containing the gold cores of $Au_8$, $Au_9$ and $Au_{11}$ can be chemically synthesised, deposited onto titania surfaces and treated to remove some of the ligands.[2] The use of surface XPS has proven useful to follow changes in electronic structures of these systems. This work inspired us to explore other spectroscopic techniques for identifying the breaking and formation of chemical bonds that are expected to occur following cluster preparation, deposition and activation on a surface.

Infra-red spectroscopy is commonly used to observe the vibrational frequencies of key functional groups to monitor changes in chemical bonding during chemical synthesis. Despite recent, yet significant attention of the scientific community to chemical synthesis and characterisation of atomically precise gold-containing clusters (both thiol- and phosphine-protected), detailed IR studies of these systems are missing in the literature. This could be due to significant difficulties associated with acquisition of high-quality data across a wide range of frequencies necessary for detailed investigation. As pointed out by Stellwagen *et al.*, "the Au–S related peaks lie at even lower energies (220 $cm^{-1}$), and fall outside the range of our FT-IR spectrometer. In general the Au–S vibrations are very weak and difficult to observe".[3] Other relevant literature reports have

[a]*Department of Chemistry, University of Adelaide, South Australia 5005, Australia. E-mail: greg.metha@adelaide.edu.au; Fax: +61 8 8303 4358; Tel: +61 8 8303 5943*
[b]*The MacDiarmid Institute for Advanced Materials and Nanotechnology, Department of Chemistry, University of Canterbury, Christchurch 8140, New Zealand*
[c]*Chemistry Department, University of Malaya, 50603 Kuala Lumpur, Malaysia*
[d]*Australian Synchrotron, 800 Blackburn Road, Clayton, Vic 3168, Australia*
[e]*School of Chemical & Physical Sciences, Flinders University, G.P.O. Box 2100, Adelaide, South Australia 5001, Australia*

† Electronic supplementary information (ESI) available. See DOI: 10.1039/c3ra44803g



This journal is © The Royal Society of Chemistry 2013

Open Access Article. Published on 11 September 2013. Downloaded on 1/20/2026 10:47:54 PM.
This article is licensed under a Creative Commons Attribution 3.0 Unported Licence.

focused on FTIR investigations of Au–S vibrations for much larger (>1.5 nm), thiolate protected gold nanoparticles, where the metal cores were not defined with atomic precision.[4,5] Smaller clusters (up to 40 Au atoms) were shown to have intense optical activity due to metal-based transitions in the near-infrared region.[6] Earlier infra-red studies of chemically-synthesised, atomically precise ultra-small metal clusters indicate that strong metal–ligand bond vibrations appear at 450 $cm^{-1}$ for phosphine-stabilised clusters.[7] At the same time, higher frequency modes associated with uncoordinated counter-ions were also observed. For example, in the case of $Au_8Pt(PPh_3)_8(NO_3)_2$ the band at 1360 $cm^{-1}$ was assigned to $NO_3^-$.[7] Lower frequency bands (*i.e.* <400 $cm^{-1}$) have been observed in earlier studies of metal cluster carbonyl clusters (*e.g.* $Ru_3(CO)_{12}$) but these features were not generally attributed to specific modes except in a few highly symmetric cases.[8] These low frequency modes are generally expected to involve vibrational motions of the cluster core which will be very weak in intensity.

Recently, Fielicke and co-workers have applied IR-action spectroscopy using the FELIX tuneable IR-free electron laser to reveal low frequency vibrations of size-specific metal clusters produced in the gas phase by laser ablation. Multiple IR photons are used to resonantly dissociate rare gas atoms (usually Ar or Kr) attached to anionic, neutral and cationic clusters prepared under supersonically-cooled molecular beam conditions. Detection by time-of-flight mass spectrometry allows unambiguous spectral assignments to specifically-sized metal clusters. In combination with Density Functional Theory (DFT) calculations, these workers have been able to identify IR-active cluster vibrations. In cases where two or more isomers are feasible, it has been possible to correlate the observed spectral features to a specific isomer, or isomers. Pertinent examples include $Au_7$, $Au_{19}$ and $Au_{20}$,[9] and Y-doped Au clusters.[10–12]

Inspired by the possibility of identifying low frequency vibrational modes of ligand-stabilised clusters by comparison with DFT calculations, we have undertaken the measurement of low intensity, low frequency vibrational modes of chemically-synthesised, atomically-precise ligand-stabilised metal clusters using a high intensity synchrotron-based far-IR source. Herein we report a methodology for obtaining reproducible spectra of ligand-protected clusters, which has been developed over several visits to the Far-IR beamline at the Australian Synchrotron. We have focused on the gold cluster cores of $Au_6$, $Au_8$, $Au_9$ and $Au_6Pd$ stabilised by phenylphosphine-based ligands. The experimentally obtained spectra are compared with DFT-computed vibrational frequency calculations of the full cluster, including all ligands. This allows us to identify key features in the IR spectrum that can be assigned to specific vibrational motions of the metal core, as well as vibrations between the metal atoms and ligands (*i.e.* Au–P bonds). We note the very recent report of a DFT investigation of thiol protected, size specific gold clusters showing calculated IR and Raman spectra for the clusters $Au_4$.[13]

## Experimental & computational procedures

The $Au_6(Ph_2P(CH_2)_3PPh_2)_4(NO_3)_2$ cluster (CSD Refcode BOTSOS; hereafter referred to $Au_6$) was prepared according to the procedure reported by Van der Velden *et al.*[14] The $Au_8(PPh_3)_8(NO_3)_2$ cluster (CSD Refcode OPAUPF; hereafter referred to $Au_8$) was synthesised following protocol described by Van der Velden *et al.*[15] The $Au_9(PPh_3)_8(NO_3)_3$ cluster (CSD Refcode MIVPOX; hereafter referred to $Au_9$) was prepared following the method described by Wen *et al.*[16] The $Pd(PPh_3)Au_6(PPh_3)_6(NO_3)_2$ cluster (CSD Refcode UHIPEG; hereafter referred to $Au_6Pd$) was prepared following the procedure of Takata *et al.*,[17] which gives higher yield of this cluster than earlier reported (along with its crystal structure) by Quintilio *et al.*[18] Note that for the $Au_6Pd$ cluster, the crystal structure utilised referred to the similar $Pd(PPh_3)Au_6(PPh_3)_6(PF_6)_2$, which employs a $PF_6^-$ counter-ion, however this is not expected to have affected the cluster geometry given the omission of counter-ions in the calculation.

Samples were prepared by pressing 50 mg of pure powdered cluster material into a pellet. Their far-IR absorption spectra were recorded using the IFS125 Bruker FT spectrometer located at the Far-IR beamline, at the Australian Synchrotron. The transmission spectrum for each sample was recorded from 50 to 650 $cm^{-1}$, at 1 $cm^{-1}$ resolution utilising the synchrotron light source (200 mA in top-up mode), a 6 micron thick multilayer Mylar beamsplitter in combination with a Si bolometer detector; the bolometer was equipped with a 800 $cm^{-1}$ far-IR cut-on cold-filter consisting of a 13 micron PE film overlaid with 6 micron diamond scatter layer. Samples were recorded at room temperature and again at 77 K with no discernible differences between spectra; all spectra were baseline corrected.

Geometry optimisation and harmonic vibrational frequency calculations of the gold cluster compounds, including all ligands, were undertaken using the M06 density functional[19] in the Gaussian 09 suite of programs.[20] Starting geometries were taken from crystal structures obtained from X-ray diffraction patterns of the synthesised clusters (reported earlier by others or ourselves) which were deposited in the Cambridge Crystallographic Database.[21] All counter ions were removed, with the appropriate number of electrons removed from the calculations to balance the charge. All atoms were treated using the LanL2DZ basis set and related Effective Core Potentials (ECP).[22–25] All optimisations were

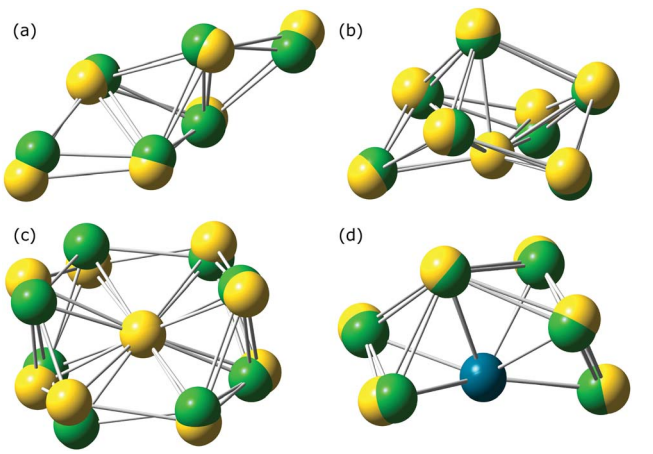


**Fig. 1** X-ray crystal structures (green) and DFT optimised structures (yellow) for the (a) $Au_6$, (b) $Au_8$, (c) $Au_9$, and (d) $Au_6Pd$ clusters. Ligand groups are omitted for clarity.

Open Access Article. Published on 11 September 2013. Downloaded on 1/20/2026 10:47:54 PM.
This article is licensed under a Creative Commons Attribution 3.0 Unported Licence.

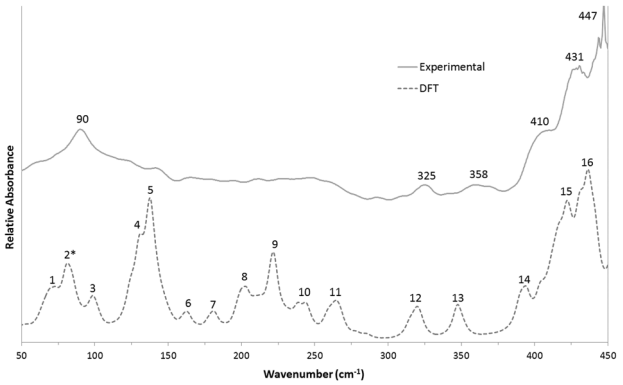


**Fig. 2** Experimental (solid line) and simulated (dotted line) far-IR spectrum of the $Au_6$ cluster.

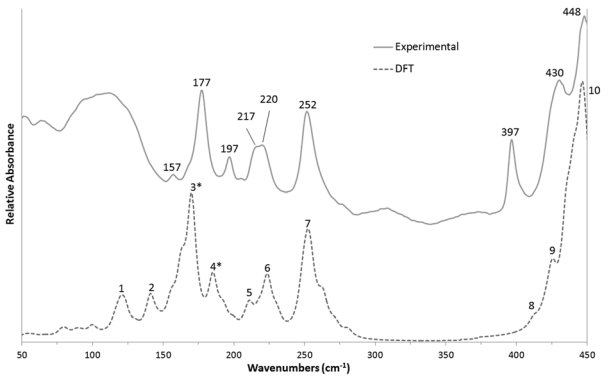


**Fig. 4** Experimental (solid line) and simulated (dotted line) far-IR spectrum of the $Au_9$ cluster.

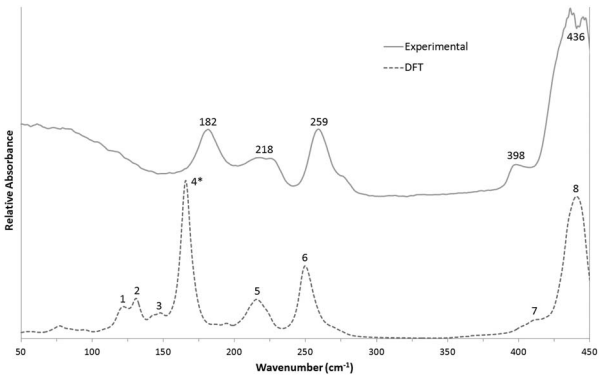


**Fig. 3** Experimental (solid line) and simulated (dotted line) far-IR spectrum of the $Au_8$ cluster.

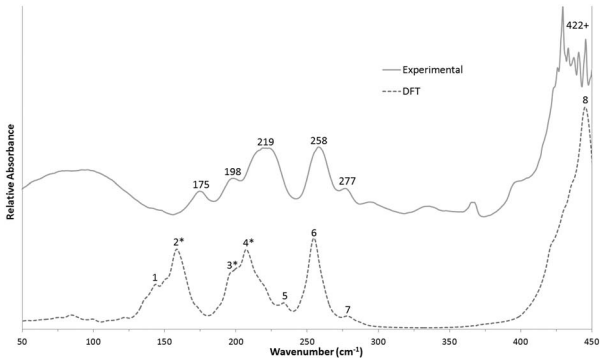


**Fig. 5** Experimental (solid line) and simulated (dotted line) far-IR spectrum of the $Au_6Pd$ cluster.

performed with no symmetry constraints, *i.e.* in the $C_1$ point group. Each optimised geometry was followed by a harmonic frequency calculation to confirm that the geometry was a true minimum with no imaginary frequencies. The exception to this was the $Au_8$ structure, which was optimised to a stationary point with three low-frequency imaginary frequencies (42.6, 30.8, and 26.1 $cm^{-1}$). Inspection of the imaginary modes reveal that they correspond to slight rotations of phenyl groups and despite numerous attempts at re-optimisation using finer grid sizes and alternative minimisation algorithms we were unable to eliminate them. In light of the small magnitude and local nature of these vibrations, we conclude that they do not adversely impact on our assessment of the core cluster vibrations which are of primary interest here. To obtain the predicted IR spectra, each stick spectrum is convoluted with a Gaussian line shape function with 8 $cm^{-1}$ full width at half maximum using the GaussView 5 program. Full geometric information for each optimised structure is provided in the accompanying ESI file.†

## Results & discussion

The optimised structures for the cluster compounds of $Au_6$, $Au_8$, $Au_9$, and $Au_6Pd$ are shown in Fig. 1, with only Au and Pd atoms shown for clarity. Superimposed on these structures are the corresponding crystal structures. The superimposed structures presented in Fig. 1 illustrate the very close match between "gas-phase" and condensed phase geometries. There is a trend across all molecules towards longer bond lengths, as the molecule is optimised from the crystal structure starting position, to its final gas-phase geometric minima.

The predicted spectra over the range 50–450 $cm^{-1}$ for the $Au_6$, $Au_8$, $Au_9$ and $Au_6Pd$ clusters are shown in Fig. 2–5 as dotted lines. Note that these spectra only include the calculated fundamental vibrations and so do not include overtones or combination bands. The number of calculated transitions is vast, with more than 150 transitions occurring in the region presented above. Given the large number of vibrations to consider, Tables 1–4 list the calculated frequency modes up to 450 $cm^{-1}$ that pass one of two selection criteria. Firstly, in order to distinguish the normal modes involving the cluster core vibrations from other low frequency modes, we have identified the normal coordinate motions that involve significant motion of the Au, Pd, and P atoms. These appear in Tables 1–4 as a percentage of the total non-mass-weighted atomic motion (*i.e.* %Au and %P). Secondly, the tables include any normal mode that has significant calculated IR intensity of >1 km $mol^{-1}$. These modes are listed either individually or as groups of peaks and numbered sequentially starting at low energy. This peak numbering scheme in Tables 1–4 is the same as the one used in the simulated spectra presented in Fig. 2–5. For the calculated

 This journal is © The Royal Society of Chemistry 2013

Open Access Article. Published on 11 September 2013. Downloaded on 1/20/2026 10:47:54 PM.
This article is licensed under a Creative Commons Attribution 3.0 Unported Licence.

**Table 1** Summary of all calculated contributing transitions for the $Au_6$ cluster and their assignment to the predicted spectral peaks, as well as their assignment to the observed far-IR spectrum of the cluster, and a brief description of the assigned transition modes

| # | Peak ($cm^{-1}$) | Contributing vibrations ($cm^{-1}$) | IR intensity (km $mol^{-1}$) | %Au motion | %P motion | Assigned ($cm^{-1}$) | Mode description |
|---|---|---|---|---|---|---|---|
| 1 | 73 | 69.6 | 1.3 | 6.1% | 4.8% | | |
| | | 72.9 | 1.4 | 8.7% | 4.6% | | |
| 2 | 81 | 80.4* | 4.7 | 17.1% | 5.1% | 90.2 | Au core distortion |
| | | 81.1 | 1.1 | 8.6% | 6.3% | | |
| | | 84.1* | 4.3 | 16.4% | 6.6% | | |
| | | 87.9 | 0.8 | 16.8% | 5.0% | | |
| 3 | 99 | 98.8 | 3.7 | 5.6% | 5.4% | | |
| | | 104.9 | 0.1 | 14.5% | 5.7% | | |
| 4 | 131 | 129.9 | 3.6 | 3.4% | 7.3% | | |
| | | 130.5 | 6.1 | 4.9% | 6.6% | | |
| 5 | 138 | 137.2 | 5.3 | 4.8% | 5.9% | | |
| | | 137.9 | 9.6 | 6.7% | 7.0% | | |
| | | 139.0 | 1.8 | 4.3% | 7.4% | | |
| | | 142.8 | 2.9 | 6.1% | 6.9% | | |
| 6 | 163 | 162.6 | 1.3 | 1.9% | 4.0% | | |
| | | 163.9 | 1.1 | 13.3% | 4.6% | | |
| 7 | 180 | 179.8 | 1.1 | 2.2% | 3.3% | | |
| | | 181.8 | 2.0 | 1.3% | 3.0% | | |
| 8 | 203 | 198.3 | 1.9 | 0.0% | 2.8% | | |
| | | 200.1 | 2.3 | 0.8% | 1.8% | | |
| | | 203.5 | 3.7 | 0.7% | 2.1% | | |
| 9 | 222 | 219.3 | 1.5 | 0.0% | 1.4% | | |
| | | 220.9 | 1.3 | 0.0% | 1.2% | | |
| | | 222.0 | 7.8 | 0.0% | 1.4% | | |
| 10 | 244 | 238.5 | 2.9 | 0.0% | 1.4% | | |
| | | 244.2 | 3.6 | 0.0% | 1.6% | | |
| 11 | 265 | 263.3 | 1.0 | 0.0% | 1.5% | | |
| | | 264.2 | 1.1 | 0.0% | 2.0% | | |
| | | 265.3 | 1.1 | 0.0% | 1.9% | | |
| 12 | 320 | 314.8 | 1.7 | 0.0% | 7.3% | 325.4 | $P_2Ph_4$–$(CH_3)_3$ wag – ligand 1 |
| | | 318.9 | 1.5 | 0.0% | 8.0% | | $P_2Ph_4$–$(CH_3)_3$ wag – ligand 2 |
| | | 319.9 | 1.4 | 0.7% | 9.4% | | $P_2Ph_4$–$(CH_3)_3$ wag – ligand 3 |
| | | 321.7 | 1.9 | 0.0% | 8.2% | | $P_2Ph_4$–$(CH_3)_3$ wag – ligand 4 |
| 13 | 348 | 347.2 | 3.4 | 0.0% | 10.7% | 357.7 | P–$(CH_2)_3$–P distortion |
| | | 347.8 | 1.3 | 0.0% | 11.4% | | |
| 14 | 394 | 390.0 | 3.6 | 0.9% | 15.1% | 410.3 | P–C–C–C–P bend |
| | | 394.3 | 4.2 | 0.8% | 15.1% | | |
| 15 | 422 | 421.7 | 4.9 | 0.5% | 13.2% | 430.5 | Au–P stretch |
| | | 422.3 | 4.6 | 0.0% | 11.1% | | P–Ph stretch |
| 16 | 436 | 429.8 | 5.2 | 1.2% | 16.3% | 446.9 | Au–P stretch |
| | | 431.3 | 6.3 | 1.2% | 16.5% | | Au–P stretch |
| | | 436.4 | 14.6 | 0.0% | 16.6% | | P–Ph stretch |
| | | 441.0 | 7.7 | 0.8% | 17.0% | | P–Ph stretch |

transitions that are assigned to experimental features, a brief description of the normal mode also appears in Tables 1–4. For each cluster, several key, core vibrations involving the metal atoms are pictorially represented in Fig. 6–9, and the peaks corresponding to these transitions are highlighted within Fig. 2–5 as well as Tables 1–4 with an asterisk.

Open Access Article. Published on 11 September 2013. Downloaded on 1/20/2026 10:47:54 PM.
This article is licensed under a Creative Commons Attribution 3.0 Unported Licence.

**Table 2** Summary of all calculated contributing transitions for the $Au_8$ cluster and their assignment to the predicted spectral peaks, as well as their assignment to the observed far-IR spectrum of the cluster, and a brief description of the assigned transition modes

| # | Peak ($cm^{-1}$) | Contributing vibrations ($cm^{-1}$) | IR intensity (km $mol^{-1}$) | %Au motion | %P motion | Assigned ($cm^{-1}$) | Mode description |
|---|---|---|---|---|---|---|---|
| 1 | 122 | 119.1 | 3.4 | 5.2% | 4.6% | | |
| | | 121.1 | 1.7 | 3.8% | 3.9% | | |
| | | 122.2 | 2.0 | 3.2% | 3.5% | | |
| | | 124.4 | 1.9 | 4.8% | 4.3% | | |
| 2 | 131 | 131.1 | 9.3 | 7.5% | 5.6% | | |
| 3 | 148 | 142.6 | 2.9 | 10.7% | 5.2% | | |
| | | 147.4 | 1.7 | 12.7% | 5.0% | | |
| | | 148.7 | 1.9 | 12.6% | 4.8% | | |
| 4 | 166 | 165.1* | 23.9 | 20.3% | 2.7% | 181.8 | Au core distortion |
| | | 166.4* | 23.9 | 20.2% | 2.9% | | |
| | | 171.6 | 3.2 | 16.7% | 1.6% | | |
| 5 | 216 | 210.3 | 1.5 | 0.0% | 0.8% | 217.9 | Ph rock |
| | | 210.9 | 1.7 | 0.0% | 1.4% | | |
| | | 214.5 | 2.8 | 0.0% | 1.2% | | |
| | | 215.8 | 1.2 | 0.0% | 1.3% | | |
| | | 217.0 | 1.6 | 0.5% | 1.5% | | |
| | | 219.1 | 1.8 | 0.0% | 1.3% | | |
| 6 | 250 | 247.4 | 4.1 | 0.0% | 1.1% | 258.9 | Ph rock |
| | | 248.3 | 3.8 | 0.0% | 0.9% | | |
| | | 249.4 | 4.1 | 0.0% | 1.2% | | |
| | | 249.9 | 3.3 | 0.0% | 1.3% | | |
| | | 250.2 | 1.7 | 0.0% | 1.4% | | |
| | | 251.7 | 3.1 | 0.0% | 1.0% | | |
| | | 253.1 | 3.9 | 0.0% | 1.3% | | |
| 7 | 411 (shoulder) | 410.5 | 0.5 | 0.0% | 1.9% | 398.2 | Ph twist |
| | | 411.5 | 0.4 | 0.0% | 0.7% | | |
| 8 | 441 | 428.9–445.8 | Avg. 3.9 | Avg. 0% | Avg. 13% | 436.3 | $PPh_3$ distortion |

Also shown in Fig. 2–5 are the experimental IR spectra for $Au_6$, $Au_8$, $Au_9$ and $Au_6Pd$ (solid line). All clusters exhibit an intense absorption near 440 $cm^{-1}$ and a broad featureless absorption below 130 $cm^{-1}$, except $Au_6$ which has a feature ~90 $cm^{-1}$. We are confident that the spectrometer is operating correctly in this region since we were able to observe characteristic features present in this region for the mono-gold compound ($AuPPh_3Cl$) which were in agreement with earlier reported data.[26] The spectrum of $AuPPh_3Cl$ (see Fig. S1 in ESI†) was recorded under similar conditions to other spectra in this study, confirming that the instrumentation set-up is capable of data acquisition in this region. The spectrum shows very little difference when recorded under reduced temperature conditions (77 K) thus removing the possibility of phonon bands being confused for features due to molecular vibrations. Nevertheless, it seems likely that the broad features arise from dampening of the low frequency vibrations due to the condensed phase nature of the sample as the calculated spectrum is generated under gas phase (*i.e.* isolated molecule) conditions.

The $Au_8$, $Au_9$ and $Au_6Pd$ spectra also display several distinct peaks between 180 and 260 $cm^{-1}$. The higher energy feature at 430 $cm^{-1}$ has been previously observed in the pure ligand, $PPh_3$, and identified as being due to P–$Ph_3$ vibrations.[27] This is consistent with our calculations, although we also show that Au–P stretches occur in the same spectral region (*vide infra*). Some of the intense features near 450 $cm^{-1}$ for $Au_6$, $Au_8$ and $Au_6Pd$ reach 100% absorption but no attempt was made to reduce the concentration due to the low significance of this spectral region.

To the best of our knowledge, the detailed far-IR spectra below 300 $cm^{-1}$ reported here are the first ever high quality dataset for chemically synthesised, atomically precise gold clusters, enabling detailed analysis of their features. Discussed below are the assignments made for each of the observed peaks, which are based upon calculated vibrational frequencies and predicted intensities (Tables 1–4).

### A. The $Au_6$ cluster

The experimental $Au_6$ spectrum (Fig. 2) clearly consists of two main peaks (including a shoulder) above 400 $cm^{-1}$, as well as a broad peak centred at 90 $cm^{-1}$. The former peaks closely match the calculated spectrum, which predicts three transitions at

 This journal is © The Royal Society of Chemistry 2013

Open Access Article. Published on 11 September 2013. Downloaded on 1/20/2026 10:47:54 PM.
This article is licensed under a Creative Commons Attribution 3.0 Unported Licence.

**Table 3** Summary of all calculated contributing transitions for the $Au_9$ cluster and their assignment to the predicted spectral peaks, as well as their assignment to the observed far-IR spectrum of the cluster, and a brief description of the assigned transition modes

| # | Peak ($cm^{-1}$) | Contributing vibrations ($cm^{-1}$) | IR intensity (km $mol^{-1}$) | %Au motion | %P motion | Assigned ($cm^{-1}$) | Mode description |
|---|---|---|---|---|---|---|---|
| 1 | 121 | 116.0 | 2.1 | 1.9% | 1.7% | | |
| | | 119.3 | 2.7 | 6.0% | 2.4% | | |
| | | 120.0 | 2.0 | 5.6% | 2.3% | | |
| | | 122.9 | 4.6 | 3.6% | 1.7% | | |
| 2 | 141 | 140.9 | 7.2 | 8.3% | 5.8% | 157.2 | Au core distortion |
| 3 | 170 | 162.8 | 11.2 | 8.1% | 4.6% | 177.4 | Au core distortion |
| | | 170.1* | 28.0 | 17.7% | 3.3% | | |
| 4 | 185 | 185.2* | 11.2 | 17.7% | 1.7% | 196.7 | Au core distortion |
| 5 | 211 | 210.7 | 2.0 | 0.0% | 1.1% | 216.5 | Ph rock |
| | | 211.0 | 3.2 | 0.0% | 0.8% | | |
| 6 | 224 | 217.6 | 2.7 | 0.0% | 1.2% | 219.8 | Ph rock |
| | | 222.2 | 2.3 | 0.0% | 0.7% | | |
| | | 223.7 | 5.6 | 0.0% | 0.7% | | |
| | | 224.2 | 3.1 | 0.0% | 1.4% | | |
| 7 | 253 | 248.9 | 6.6 | 0.0% | 1.0% | 251.7 | $PPh_3$ distortion |
| | | 251.6 | 6.2 | 0.0% | 0.8% | | |
| | | 252.2 | 3.2 | 0.0% | 0.6% | | |
| | | 253.9 | 9.9 | 0.0% | 0.9% | | |
| 8 | 411 (shoulder) | 411.8 | 0.9 | 0.0% | 1.0% | 396.8 | Ph twist |
| | | 412.2 | 0.7 | 0.0% | 1.0% | | |
| 9 | 426 | 424.5 | 1.5 | 0.0% | 3.2% | 430.0 | Ph twist |
| | | 424.6 | 1.9 | 0.0% | 3.0% | | |
| | | 425.4 | 3.6 | 0.0% | 4.7% | | |
| | | 425.5 | 1.9 | 0.0% | 2.5% | | |
| 10 | 447 | 435.2–448.8 | Avg. 8.1 | Avg. 0% | Avg. 13% | 447.9 | $PPh_3$ distortion |

393.7 $cm^{-1}$ (#14) due to P–$(CH_2)_3$–P bending, at 422.3 $cm^{-1}$ and 436.3 $cm^{-1}$ (#15 & #16 respectively) both due to a combination of the Au–P and P–$Ph_3$ stretches.

The observed peak at 90 $cm^{-1}$ corresponds to a group of calculated transitions around 84 $cm^{-1}$ (#2), which are all due to metal core vibrations. All four transitions have significant Au motions of 9–17% (see Table 1) and the displacement vectors for the two most IR intense vibrations are shown in Fig. 6. This low frequency peak at 90 $cm^{-1}$ is interesting since none of the other clusters have observable, nor calculated, core metal vibrational modes this low in frequency. The simulated spectrum also shows a strong peak with a shoulder at 138 $cm^{-1}$ and 131 $cm^{-1}$, respectively (#5 & #4), both of which consist of several modes with moderate %Au motions (~5%) and significant IR intensities ($A$ = 4–10). These peaks match the two shoulders (unlabelled) in the experimental spectrum near 120 and 148 $cm^{-1}$.

The experimental spectrum also shows two weaker peaks at 325 $cm^{-1}$ and 358 $cm^{-1}$. These also appear in the calculated spectrum at 320 $cm^{-1}$ (#12) and 348 $cm^{-1}$ (#13) respectively, and correspond to distortions of the chelating P–$(CH_2)_3$–P ligands. The simulated spectra also show a number of peaks (#6–11) in the region from 160 $cm^{-1}$ to 265 $cm^{-1}$, which do not distinctly appear in the experimental spectrum. Only one of these transitions contains significant Au motion (#6 with 13% Au), with a low IR intensity (~1.1 km $mol^{-1}$), and the remainder are large-amplitude ligand vibrations. There are other transitions (<150 $cm^{-1}$) involving large amplitude motions spanning several ligand groups, that are calculated to have non-negligible IR intensities but do not appear in the spectrum. We suggest that given the condensed nature of the samples (*i.e.* pressed pellet) that these modes are more readily quenched than the core metal vibrations. Although we have no direct evidence for this, it is a common theme observed for all the other clusters (*vide infra*).

### B. The $Au_8$ and $Au_9$ clusters

Both the $Au_8$ and $Au_9$ spectra display an intense peak at 440 $cm^{-1}$. These features are clearly reproduced in the associated simulated spectra. As mentioned above, the normal mode analysis indicates that these transitions ((#8) in the case of $Au_8$ and (#10) for $Au_9$) correspond to the P–$Ph_3$ stretching vibrations

Open Access Article. Published on 11 September 2013. Downloaded on 1/20/2026 10:47:54 PM.
This article is licensed under a Creative Commons Attribution 3.0 Unported Licence.

**Table 4** Summary of all calculated contributing transitions for the $Au_6Pd$ cluster and their assignment to the predicted spectral peaks, as well as their assignment to the observed far-IR spectrum of the cluster, and a brief description of the assigned transition modes

| # | Peak ($cm^{-1}$) | Contributing vibrations ($cm^{-1}$) | IR intensity (km $mol^{-1}$) | %Au motion | %Pd motion | %P motion | Assigned ($cm^{-1}$) | Mode description |
|---|---|---|---|---|---|---|---|---|
| 1 | 144 | 135.7 | 2.6 | 2.8% | 2.6% | 4.1% | | |
| | | 139.7 | 1.6 | 2.7% | 1.5% | 2.1% | | |
| | | 142.3 | 1.4 | 3.3% | 0.7% | 2.1% | | |
| | | 143.9 | 3.9 | 3.8% | 2.4% | 2.4% | | |
| 2 | 159 | 149.7 | 3.4 | 5.3% | 2.7% | 3.9% | 174.5 | Pd–Au–P stretch |
| | | 150.9 | 1.5 | 5.6% | 0.7% | 3.2% | | P–Au–Au–P stretch |
| | | 156.0 | 2.2 | 5.8% | 0.8% | 2.6% | | Metal core distortion |
| | | 157.1 | 4.1 | 6.8% | 0.7% | 4.0% | | Pd–Au–P stretch |
| | | 158.9* | 6.5 | 7.7% | 1.1% | 3.8% | | Metal core distortion |
| | | 162.2 | 5.2 | 8.3% | 1.9% | 3.7% | | P–Au–Au–P stretch |
| 3 | 195 (shoulder) | 195.2* | 6.0 | 4.7% | 2.5% | 1.8% | 197.7 | Metal core distortion |
| | | 198.9 | 1.5 | 1.3% | 1.4% | 2.2% | | $PPh_3$ rotation |
| | | 200.8 | 1.8 | 4.8% | 2.0% | 1.9% | | Pd–P stretch |
| 4 | 207 | 201.1 | 2.6 | 1.9% | 1.6% | 1.8% | 218.9 | $PPh_3$ rotation |
| | | 206.7* | 9.0 | 8.0% | 4.9% | 1.0% | | Metal core distortion |
| | | 210.1 | 3.7 | 0.5% | 1.0% | 1.5% | | Ph rock |
| | | 211.2 | 1.7 | 2.6% | 1.4% | 1.1% | | $PPh_3$ rotation |
| | | 214.5 | 1.5 | 8.4% | 8.5% | 1.8% | | Pd–P stretch |
| 5 | 234 | 233.8 | 2.1 | 0.0% | 0.0% | 0.9% | | Ph rock |
| 6 | 255 | 252.1 | 3.1 | 0.0% | 0.0% | 1.0% | 257.9 | Ph rock |
| | | 253.5 | 3.2 | 0.0% | 0.0% | 1.1% | | |
| | | 254.3 | 4.2 | 0.0% | 0.0% | 1.1% | | |
| | | 254.9 | 1.4 | 0.4% | 0.3% | 1.7% | | |
| | | 255.7 | 3.3 | 0.0% | 0.4% | 1.9% | | |
| | | 256.8 | 3.8 | 0.0% | 0.0% | 1.3% | | |
| | | 260.6 | 2.5 | 0.0% | 0.0% | 0.6% | | |
| 7 | 278 | 277.6 | 0.7 | 0.0% | 0.0% | 1.0% | 276.7 | Ph rotation |
| | | 279.6 | 0.4 | 0.0% | 0.0% | 1.3% | | |
| 8 | 445 | 421.1–449.2 | Avg. 4.6 | Avg. 0% | Avg. 0% | Avg. 11% | 400–450+ | $PPh_3$ distortion |

with their high intensity arising from the large number of similar bonds – there are eight $PPh_3$ ligands per cluster core each giving rise to three P–Ph vibrations. The shoulder at 430 $cm^{-1}$ in $Au_9$ matches a set of four similar transitions involving Ph-twisting vibrations (#9).

Both spectra exhibit distinct peaks at 398 $cm^{-1}$, which is much stronger in $Au_9$ compared to $Au_8$. Our calculations predict weak peaks for $Au_8$ (#7) and $Au_9$ (#8) that seem to match the position of this experimentally observed feature but not its intensity. These are due to a combination of two normal modes in each cluster, both involving phenyl group twisting vibrations. A similar mode for $Au_9$ is calculated at 426 $cm^{-1}$ (#9), which corresponds to an intense feature at 430 $cm^{-1}$ in the experimental spectrum.

The observed $Au_8$ spectrum has strong bands at 259 $cm^{-1}$ and 182 $cm^{-1}$, and a weaker, broader transition centred at 218 $cm^{-1}$. Each of these peaks is simulated with excellent fit in both relative intensity and energy. The calculated peak at 250 $cm^{-1}$ (#6), as well as the weaker peak at 216 $cm^{-1}$ (#5), are due to the rocking motions of the phenyl (Ph) group. However, the key feature in this region is the intense peak calculated at 166 $cm^{-1}$ (#4), which is attributed to the two high intensity vibrations of the gold core. Vector displacements for these intense cluster core vibrations are shown in Fig. 7. We assign these calculated vibrations to the experimentally observed peak at 182 $cm^{-1}$.

The experimental spectrum of the $Au_9$ has an intense peak at 251 $cm^{-1}$, which matches a collection of $PPh_3$ distortion modes predicted by our calculations to be around 253 $cm^{-1}$ (#7). Similarly, features observed at 217 $cm^{-1}$ and 220 $cm^{-1}$ are assigned to peaks at 211 (#5) and 224 $cm^{-1}$ (#6), respectively, both being due to $PPh_3$ rocking vibrations.

Also for $Au_9$, the peak observed at 177 $cm^{-1}$ matches the predicted peak at 170 $cm^{-1}$ (#3), and the observed feature at 197 $cm^{-1}$ matches the peak at 185 $cm^{-1}$ (#4). Both of these peaks are of particular interest too, as their origin is due to the metal core vibrations. Fig. 8 illustrates displacement vectors corresponding to these core vibrations. Our calculations predict that these features should have high intensity which is in perfect agreement with experimental data. Finally, we assign

 This journal is © The Royal Society of Chemistry 2013

Open Access Article. Published on 11 September 2013. Downloaded on 1/20/2026 10:47:54 PM.
This article is licensed under a Creative Commons Attribution 3.0 Unported Licence.

the small feature at 157 $cm^{-1}$ to the single transition peak predicted to occur at 141 $cm^{-1}$ (#2). Interestingly, this particular mode arises due to the vibration of the central Au atom (8% Au motion) relative to the ring of the other eight gold atoms around it and is calculated to have less intensity than the other gold core vibrations.

From the normal calculated mode analysis, there are two predicted transitions for the $Au_8$ cluster at 165 $cm^{-1}$ and 166 $cm^{-1}$ that involve the largest combined motion of the metal cluster core atoms (~20% Au motion). Similarly, in the case of $Au_9$ cluster there are two predicted transitions at 170 $cm^{-1}$ and 185 $cm^{-1}$ that have significant gold core motion (~18% Au motion). Importantly, the vibrational energy corresponding to the transitions responsible for these peaks is similar to that observed in the case of the gas-phase IR studies of $Au_7$–Kr cluster reported by Fielicke and co-workers.[9] Using IR-depletion spectroscopy, the authors observed three peaks at 165, 186 and 201 $cm^{-1}$, which correlated very well with their DFT-predicted spectrum (note that removal of the rare gas atom has very little effect on the vibrational frequencies of the remaining $Au_7$ cluster core). It was proposed that the cluster core (both with the Kr atom and without) has $C_s$-planar structure made up of 5 equilateral triangles and the three prominent vibrational peaks were assigned to various delocalised motions of all Au atoms in the cluster. It is interesting that the frequencies of the bare $Au_7$ cluster observed in gas phase are similar to the ones observed by us for the cores of similarly sized, chemically-synthesised gold clusters that are protected by ligands and form extended crystalline lattices. This suggests that the bonding strengths within the metal cores for these two types of cluster systems are similar, despite having quite different geometric structures (*i.e.* 3D *vs.* 2D for clusters in the gas phase).

Below 140–150 $cm^{-1}$ for both $Au_8$ and $Au_9$, the calculated spectra show a series of weaker peaks that do not resemble the experimental data. None of these are due to core cluster vibrations but involve a collection of vibrations comprising large-amplitude movement of the P–$Ph_3$ ligand groups that again, appear to be suppressed, consistent with that observed for $Au_6$.

### C. The $Au_6Pd$ cluster

This spectrum is dominated by a broad peak extending from 400 to beyond 450 $cm^{-1}$, which is assigned to a plethora of intense $PPh_3$ distortions calculated to begin at 421 $cm^{-1}$. The $Au_6Pd$ cluster is observed to have a series of strong and moderate bands at 277 (m), 258 (s), 219 (s), 198 (m) and 175 $cm^{-1}$ (m). The predicted spectrum shows a range of peaks that appear to match the experimental spectrum except they are at slightly lower energy. Calculated peaks at 278 $cm^{-1}$ (#7), 255 $cm^{-1}$ (#6) and 234 $cm^{-1}$ (#5) are due to the phenyl group

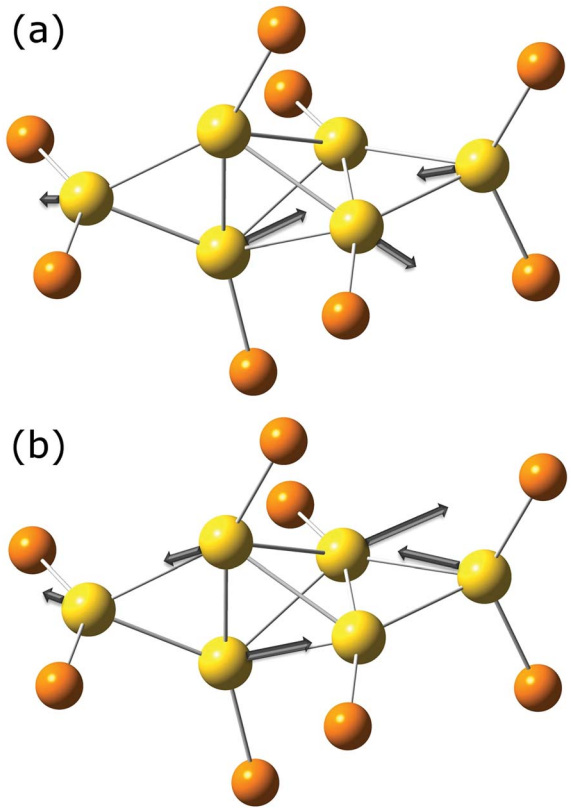


**Fig. 6** Calculated normal mode displacements associated with the cluster core vibrations for $Au_6$ at (a) 80.4 $cm^{-1}$ and (b) 84.1 $cm^{-1}$. Phenyl groups are omitted for clarity.

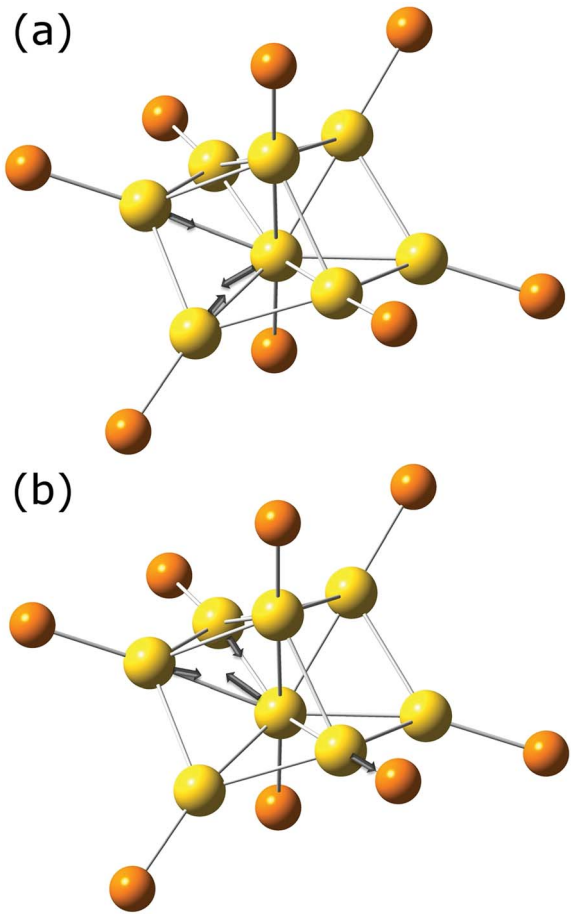


**Fig. 7** Calculated normal mode displacements associated with the cluster core vibrations for $Au_8$ at (a) 165.1 $cm^{-1}$ and (b) 166.4 $cm^{-1}$. Phenyl groups are omitted for clarity.

Open Access Article. Published on 11 September 2013. Downloaded on 1/20/2026 10:47:54 PM.
This article is licensed under a Creative Commons Attribution 3.0 Unported Licence.

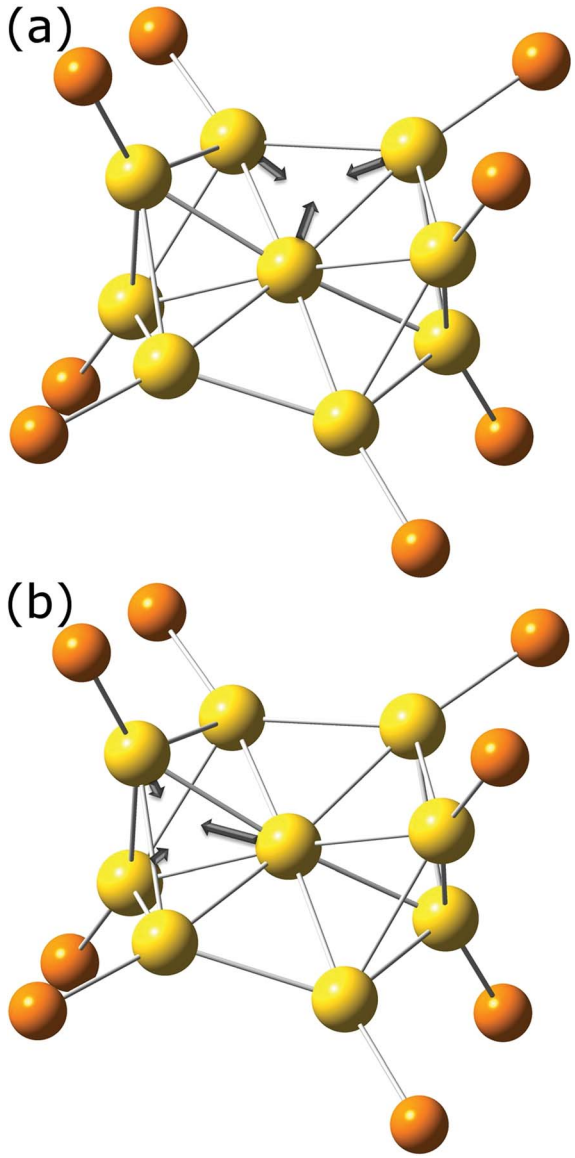


**Fig. 8** Calculated normal mode displacements associated with the cluster core vibrations for $Au_9$ at (a) 170.1 $cm^{-1}$ and (b) 185.2 $cm^{-1}$. Phenyl groups are omitted for clarity.

rotation and rocking (×2), respectively. We are assigning peaks #2, #3 and #4 to the lower energy three peaks seen in the experimentally obtained spectrum. Importantly, these vibrational modes involve a combination of Au and Pd motions. Specific transitions to note are at 159, 195 and 207 $cm^{-1}$, which have a total metal motion of >7%, with the Pd contribution ranging from 1 to 5%. The vector displacements for these modes are shown in Fig. 9. Finally, there is a weak peak experimentally observed at 360 $cm^{-1}$, which does not correlate to anything in our predicted spectrum.

We are aware of previously published FELIX IR data for a related metal cluster, namely neutral[10,11] and cationic[12] $Au_6Y$. The neutral structure is slightly distorted from planarity and this yields an IR spectrum with broad peaks from 75–220 $cm^{-1}$. The cationic structure has $C_{3v}$ symmetry and has distinct peaks at 121 and 181 $cm^{-1}$. Again, given the difference in cluster core charge and geometry, and the presence of $PPh_3$ ligands, it is surprising that the vibrational frequencies are so similar between the naked metal cluster in the gas phase and our fully ligated cluster in solid state.

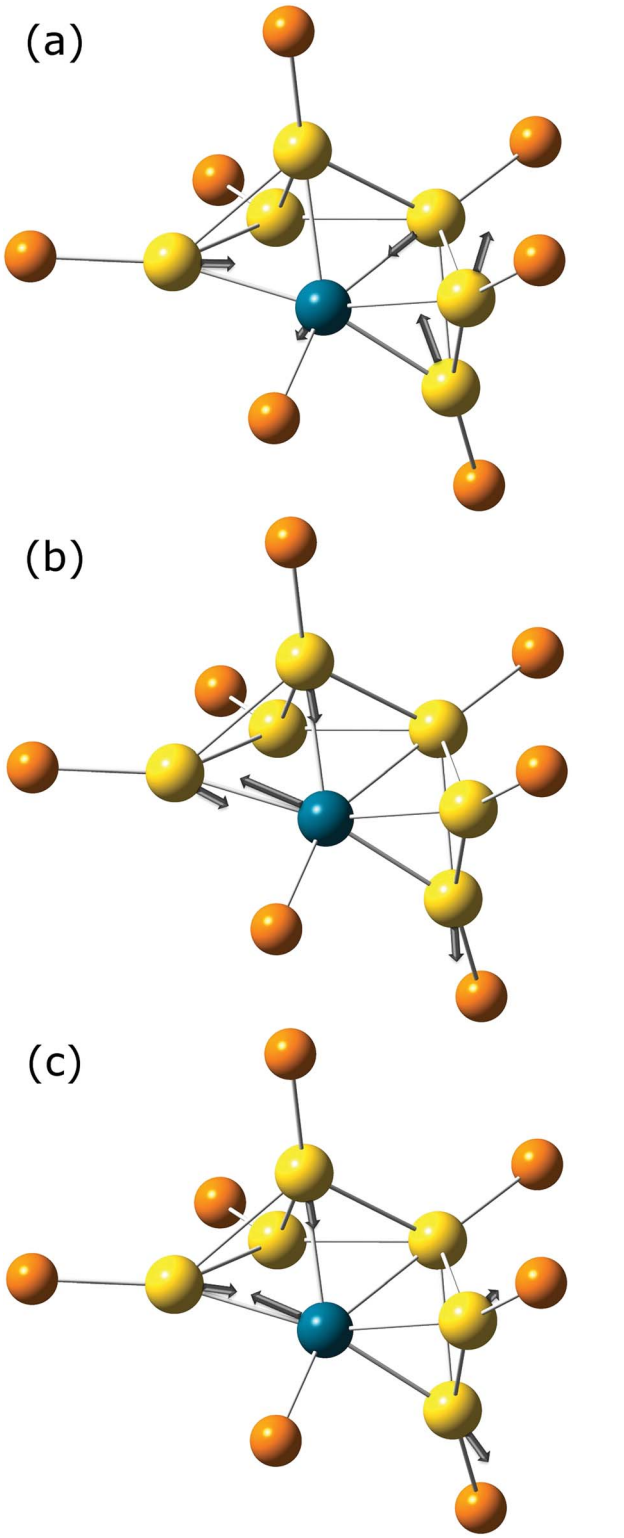


**Fig. 9** Calculated normal mode displacements associated with the cluster core vibrations for $Au_6Pd$ at (a) 158.9 $cm^{-1}$, (b) 195.2 $cm^{-1}$, and (c) 206.7 $cm^{-1}$. Phenyl groups are omitted for clarity.


This journal is © The Royal Society of Chemistry 2013

Open Access Article. Published on 11 September 2013. Downloaded on 1/20/2026 10:47:54 PM.
This article is licensed under a Creative Commons Attribution 3.0 Unported Licence.

Consistent with that observed for all three pure gold clusters reported above, the spectrum of $Au_6Pd$ is observed to contain a broad, featureless peak below 150 $cm^{-1}$, showing no resemblance to the calculated spectra. The large, multi-ligand transitions predicted to occur within this region appear to be suppressed, as postulated for the pure gold clusters above.

## Conclusions

We have demonstrated that synchrotron-based, far-IR spectroscopy can be used to identify vibrational motions of chemically-synthesised, ligand-protected pure gold and mixed-metal cluster compounds. We have identified a transition near 180 $cm^{-1}$ that involves gold cluster core vibrations for both $Au_8$ and $Au_9$. In the case of $Au_6Pd$, this transition is shifted to higher energy (218 $cm^{-1}$) implying that the presence of a Pd atom significantly affects gold cluster core *i.e.* a strong heteroatom effect is evident. The related metal core transitions in the case of $Au_6$ cluster are observed at a significantly different position (90 $cm^{-1}$) to all other clusters in this study, which do not have IR-active metal core vibrations in this region. The experimental observations have been verified by comparison with predicted IR spectra based upon DFT-optimised structures.

## Acknowledgements

This work was supported by grants from the Australian Synchrotron (AS113/HRIR/4026 and AS123/HRIR/5251). Financial support from the Centre for Energy Technologies at the University of Adelaide, the MacDiarmid Institute for Advanced Materials and Nanotechnology, the University of Canterbury and the University of Malaya is gratefully acknowledged. Computing resources provided by the National Computational Infrastructure (NCI) Facility and eResearch SA is also gratefully acknowledged. The authors also appreciate correspondence with Dr Matthew Addicoat regarding the DFT calculations.

## References

1 B. Yoon, H. Häkkinen, U. Landman, A. S. Wörz, J.-M. Antonietti, S. Abbet, K. Judai and U. Heiz, *Science*, 2005, **307**, 403–407.
2 D. P. Anderson, J. F. Alvino, A. Gentleman, H. Al Qahtani, L. Thomsen, M. I. Polson, G. F. Metha, V. B. Golovko and G. G. Andersson, *Phys. Chem. Chem. Phys.*, 2013, **15**, 3917–3929.
3 D. Stellwagen, A. Weber, G. L. Bovenkamp, R. Jin, J. Bitter and C. S. Kumar, *RSC Adv.*, 2012, **2**, 2276–2283.
4 M. J. Hostetler, J. J. Stokes and R. W. Murray, *Langmuir*, 1996, **12**, 3604–3612.
5 M. J. Hostetler, J. E. Wingate, C.-J. Zhong, J. E. Harris, R. W. Vachet, M. R. Clark, J. D. Londono, S. J. Green, J. J. Stokes, G. D. Wignall, G. L. Glish, M. D. Porter, N. D. Evans and R. W. Murray, *Langmuir*, 1998, **14**, 17–30.
6 T. G. Schaaff and R. L. Whetten, *J. Phys. Chem. B*, 2000, **104**, 2630–2641.
7 J. J. Bour, R. P. F. Kanters, P. P. J. Schlebos and J. J. Steggerda, *Recl. Trav. Chim. Pays-Bas*, 1988, **107**, 211–215.
8 D. M. Adams and I. D. Taylor, *J. Chem. Soc., Faraday Trans. 2*, 1982, **78**, 1561–1571.
9 P. Gruene, D. M. Rayner, B. Redlich, A. F. G. van der Meer, J. T. Lyon, G. Meijer and A. Fielicke, *Science*, 2008, **321**, 674–676.
10 L. Lin, P. Claes, P. Gruene, G. Meijer, A. Fielicke, M. T. Nguyen and P. Lievens, *ChemPhysChem*, 2010, **11**, 1932–1943.
11 L. Lin, T. Höltzl, P. Gruene, P. Claes, G. Meijer, A. Fielicke, P. Lievens and M. T. Nguyen, *ChemPhysChem*, 2008, **9**, 2471–2474.
12 L. Lin, P. Claes, T. Holtzl, E. Janssens, T. Wende, R. Bergmann, G. Santambrogio, G. Meijer, K. R. Asmis, M. T. Nguyen and P. Lievens, *Phys. Chem. Chem. Phys.*, 2010, **12**, 13907–13913.
13 A. Tlahuice-Flores, R. L. Whetten and M. Jose-Yacaman, *J. Phys. Chem. C*, 2013, **117**, 12191–12198.
14 J. W. A. Van der Velden, J. J. Bour, J. J. Steggerda, P. T. Beurskens, M. Roseboom and J. H. Noordik, *Inorg. Chem.*, 1982, **21**, 4321–4324.
15 J. W. A. Van der Velden, J. J. Bour, W. P. Bosman and J. H. Noordik, *Inorg. Chem.*, 1983, **22**, 1913–1918.
16 F. Wen, U. Englert, B. Gutrath and U. Simon, *Eur. J. Inorg. Chem.*, 2008, **2008**, 106–111.
17 N. H. Takata, A. M. P. Felicíssimo and V. G. Young Jr, *Inorg. Chim. Acta*, 2001, **325**, 79–84.
18 W. Quintilio, A. Sotelo and A. M. P. Felicissimo, *Spectrosc. Lett.*, 1994, **27**, 605–611.
19 Y. Zhao and D. G. Truhlar, *Theor. Chem. Acc.*, 2008, **120**, 215–241.
20 M. J. Frisch, G. W. Trucks, H. B. Schlegel, G. E. Scuseria, M. A. Robb, J. R. Cheeseman, G. Scalmani, V. Barone, B. Mennucci, G. A. Petersson, H. Nakatsuji, M. Caricato, X. Li, H. P. Hratchian, A. F. Izmaylov, J. Bloino, G. Zheng, J. L. Sonnenberg, M. Hada, M. Ehara, K. Toyota, R. Fukuda, J. Hasegawa, M. Ishida, T. Nakajima, Y. Honda, O. Kitao, H. Nakai, T. Vreven, J. A. Montgomery, J. E. Peralta, F. Ogliaro, M. Bearpark, J. J. Heyd, E. Brothers, K. N. Kudin, V. N. Staroverov, R. Kobayashi, J. Normand, K. Raghavachari, A. Rendell, J. C. Burant, S. S. Iyengar, J. Tomasi, M. Cossi, N. Rega, N. J. Millam, M. Klene, J. E. Knox, J. B. Cross, V. Bakken, C. Adamo, J. Jaramillo, R. Gomperts, R. E. Stratmann, O. Yazyev, A. J. Austin, R. Cammi, C. Pomelli, J. W. Ochterski, R. L. Martin, K. Morokuma, V. G. Zakrzewski, G. A. Voth, P. Salvador, J. J. Dannenberg, S. Dapprich, A. D. Daniels, Ö. Farkas, J. B. Foresman, J. V. Ortiz, J. Cioslowski and D. J. Fox, *Gaussian 09*, Revision **C.01**, Gaussian, Inc., Wallingford CT, 2009.
21 F. Allen, *Acta Crystallogr., Sect. B: Struct. Sci.*, 2002, **58**, 380–388.
22 T. Dunning Jr and P. Hay, *Mod. Theor. Chem.*, 1977, **3**, 1–28.
23 P. J. Hay and W. R. Wadt, *J. Chem. Phys.*, 1985, **82**, 270–283.
24 P. J. Hay and W. R. Wadt, *J. Chem. Phys.*, 1985, **82**, 299–310.
25 W. R. Wadt and P. J. Hay, *J. Chem. Phys.*, 1985, **82**, 284–298.
26 A. G. Jones and D. B. Powell, *Spectrochim. Acta, Part A*, 1974, **30**, 563–570.
27 G. B. Deacon and J. H. S. Green, *Spectrochim. Acta, Part A*, 1968, **24**, 845–852.